VSP

Advanced Composite Materials 17 (2008) 177–190

ADVANCED COMPOSITE MATERIALS
www.brill.nl/acm

Influence of Uncertainties for Compressive Buckling of Composite Materials and Its Numerical Simulations

Tetsuhiko Ueda [a,*], **Shouhei Takase** [b], **Tadashige Ikeda** [a] **and Yutaka Iwahori** [c]

[a] Department of Aerospace Engineering, Nagoya University
[b] Oji Paper Co., Ltd., Japan
[c] Advanced Composite Technology Center, Japan Aerospace Exploration Agency, Japan

Received 2 November 2007; accepted 5 December 2007

Abstract

As the first step in discussing the reliability of composite structures, a fundamental study was performed to obtain the scattering characteristics of glass–fiber reinforced plastics (GFRP) and woven carbon fiber reinforced plastics (WCFRP) as well as a reference metal. The Euler buckling load was obtained experimentally for each material. The experiments were conducted for specified rectangular specimens with simply supported edges. A new attachment to realize the simply support boundary conditions for composite materials have been prepared before these experiments. The scattering data in the results for GFRP and WCFRP composites were compared with those of a typical metal of aluminum alloy. The experimental data were also compared with numerical simulations including the uncertainties.

Keywords

Uncertainty, composite, Euler buckling, numerical simulation, GFRP, effective thickness, woven composite

1. Introduction

Recently, composite materials have provided the production base of structures in the aerospace field owing to their excellent specific strength and manufacturing flexibility for various configurations. Their potential capabilities have not yet been fully utilized however because of the difficulties with quality assurance and assessment of reliability of the products. This less than optimal utilization comes from the fact that composite materials contain more uncertainties when compared with conventional metal. Therefore, it is desired to evaluate these uncertainties more precisely to make design more effective. If we can evaluate the probabilistic characteristics

* To whom correspondence should be addressed. E-mail: ueda@nagoya-u.jp
Edited by the JSCM

DOI:10.1163/156855108X314805

even from the early designing stage, the composite can provide more reliable structures [1].

In the present paper, as the first step in discussing the reliability of composite structures, a fundamental study is performed to obtain the scattering characteristics of glass–fiber reinforced plastics (GFRP) and woven carbon–fiber reinforced plastics (WCFRP) as well as a reference metal of aluminum alloy.

Furthermore, a simulation model including uncertainties in the finite element method was studied to investigate whether it could simulate the scattering in real buckling loads. The mathematical model was used for the Monte Carlo simulation and compared with the real experimental data. In the analysis, basically linear elasticity [2] is assumed.

2. Composite and Metal Specimens

Three types of glass–fiber reinforced plastics, two types of carbon fiber reinforced plastics, and a metal are dealt with in the present study.

(1) Glass–fiber reinforced plastics (GFRP) (Hy-e E773/S2 made by Cytec Fiberite):
   (a) 0° unidirectional 8PLY denoted by L,
   (b) Pseud-isotropic [+45/0/−45/90]sym 8PLY denoted by X,
   (c) 90° unidirectional 8PLY denoted by T.

(2) Woven carbon fiber reinforced plastics (WCFRP) (W3T282 42″ F593-18, 40% made by DIC-HEXCEL) [45/0/45/0]sym 8PLY. Specimens were cut out from two plates which were supposed to have the same characteristics. However, they look different in surface appearance: WCFRP with stub denoted by A; WCFRP without stub denoted by B.

(3) Metal for a reference. Aluminum alloy 5020 (JIS H4000) denoted by M.

3. Dimensions of a Test Piece

All the test pieces were cut out from the corresponding type of uniformly 2 mm thick plates into the rectangular shape with 200 mm in length, and 12.5 mm in width. It is a prerequisite that the scattering in the dimensions of each piece should be clarified in order to evaluate the uncertainty in the structural characteristics. The thickness and the width were measured at twenty locations along the piece. The results of their measurement are listed in Tables 1 and 2, respectively. The length l, which is specified to be 200 mm, is confirmed within ± 0.2 mm error for all the pieces. Therefore, the scattering for length will be neglected in further discussions.

Table 1.
Measured width of specimens

Materials	Width b (mm)	Standard deviation σ (mm)	Coefficient of variation σ/b
FRP L	12.50	0.140	0.011
GFRP X	12.46	0.024	0.002
GFRP T	12.48	0.205	0.016
WCFRP A	12.49	0.028	0.002
WCFRP B	12.49	0.059	0.005
Metal M	12.48	0.076	0.006

Table 2.
Measured thickness of specimens

Materials	Thickness t (mm)	Standard deviation σ (mm)	Coefficient of variation σ/t
GFRP L	1.87	0.008	0.004
GFRP X	1.83	0.041	0.022
GFRP T	1.86	0.040	0.022
WCFRP A	1.78	0.003	0.002
WCFRP B	1.79	0.003	0.002
Metal M	2.00	0.009	0.005

4. Stiffness of Materials

4.1. Stiffness Tests

Before buckling experiments, stiffness tests were conducted for each material to know the uncertainty in Young's modulus. The tests for the longitudinal stiffness were first done in accordance with the JIS standard K7056 [3] by using its jigs for compression. Due to mis-tuning for set-up, the scattering in the obtained data seemed to reflect the effects of the jigs. Since the dependency on torque of guide attachment to prevent buckling was observed in the strain history, we changed the compressive tests to tensile tests. When the previous data are compared with the results of the tensile tests, their average value was 5% higher than the latter. The compressive tests displayed hysteresis during loading and unloading. Therefore, we decided to use only the tensile results for both elastic modulus and its scattering factor. This means that the same specimen was used as for the strength test which will be discussed later.

A test specimen for elastic modulus is illustrated in Fig. 1.

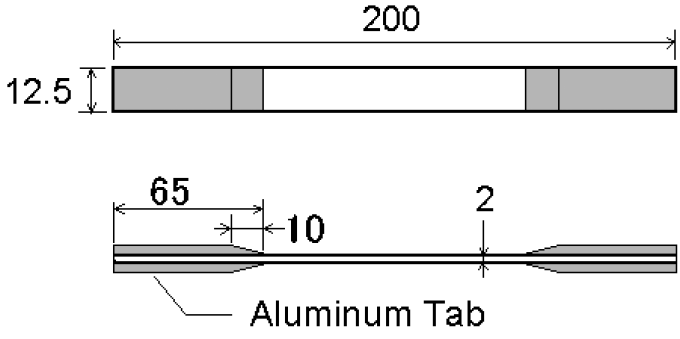

Figure 1. Test specimen for elastic modulus.

Table 3.
Measured elastic moduli

Materials	Elastic modulus E (GPa)	Standard deviation σ (GPa)	Coefficient of variation σ/E
GFRP L	48.5	0.27	0.006
GFRP X	23.9	0.07	0.003
GFRP T	12.7	0.26	0.020
WCFRP A	39.8	2.62	0.066
WCFRP B	41.1	1.64	0.040
Metal M	72.2	0.26	0.004

4.2. Stiffness Test Results

Table 3 shows the results of the stiffness tests conducted on ten pieces for each material.

The table shows each material together with its characteristics, including uncertainties. The degree of uncertainty can be found with the coefficient of variation. The coefficients of variation for Metal and GFRP X show small values whereas those for WCFRP and GFRP T are one order higher than the others. This may be attributed to the fact that WCFRP is fabric and that the elastic modulus of GFRP T is almost the same as its resin, which may be influenced by the structure of fibers.

5. Buckling Experiments

5.1. Load Attachments

It is important in buckling tests to be able to define a clear boundary condition at the edge of a test piece. In the present study, a simply supported boundary condition is adopted for buckling experiments. This was chosen because the scattering effects of the boundary may be the least among other feasible end conditions. It is difficult, however, to realize a so-called knife-edge for the composite test piece, in contrast to

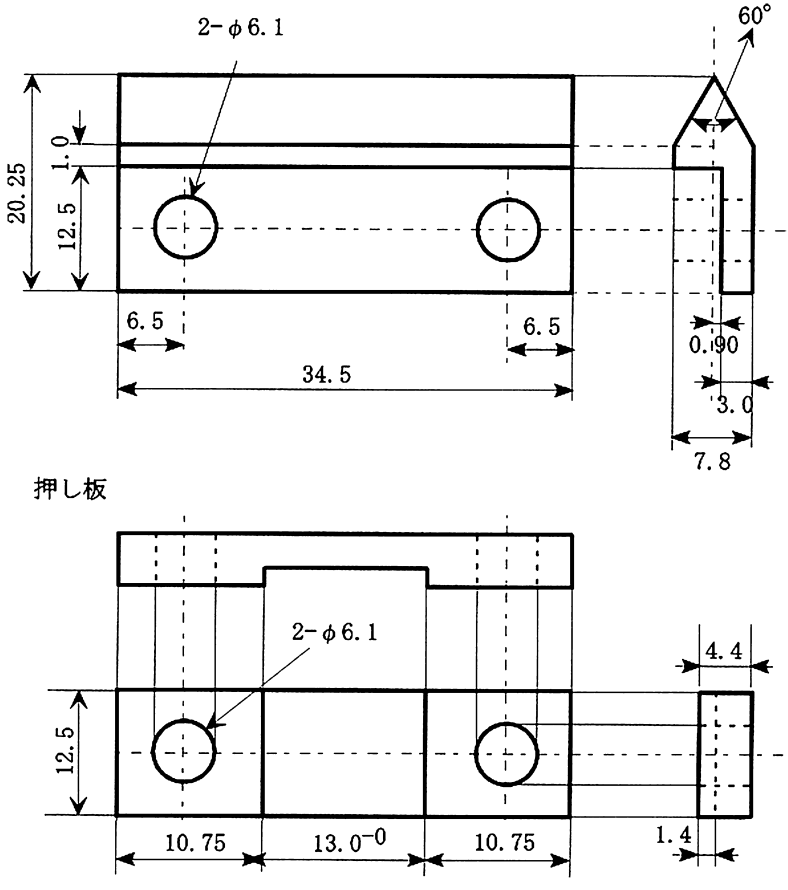

Figure 2. Edge attachment for simply supported condition.

the metal. Therefore, we newly developed an edge attachment to provide a simply supported boundary condition clearly for composite specimens. This is illustrated in Fig. 2. The parts are made of stainless steel, SUS304. This device can provide an easy setting of specimens by adjusting their edges to the guide grooves. The torque for fitting is kept constant as 80 cNM by using a hexagonal wrench. The knife-edge is placed on the cradle of the loading plate which is used for an ordinary metal knife edge. The test setup using this attachment and the measurement system are shown in Figs 3 and 4, respectively. The lateral displacement at the center of a test piece is measured by a laser sensor.

5.2. Influence of the Attachment to Buckling Loads

Because of the attachment described above, this portion increased the length of a test piece. It is obvious that the stiffness of the attachment is different from that of the specimen, which influences the buckling load. The amount of the influence was examined by the analysis using the finite element method with beam elements.

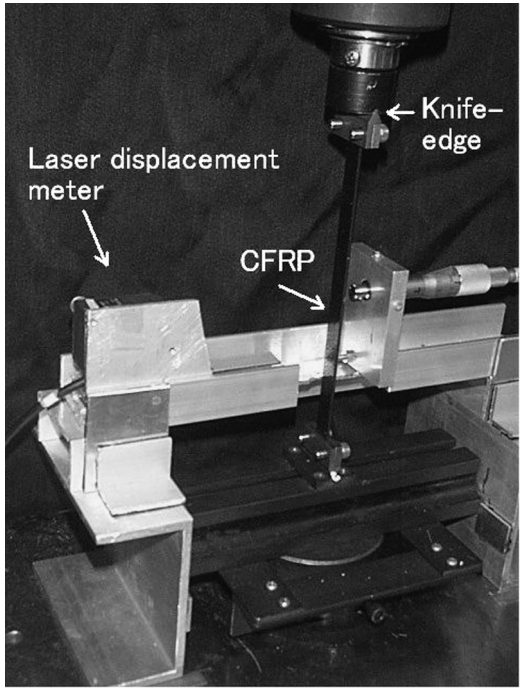

Figure 3. Setup for buckling tests with simply supported edges.

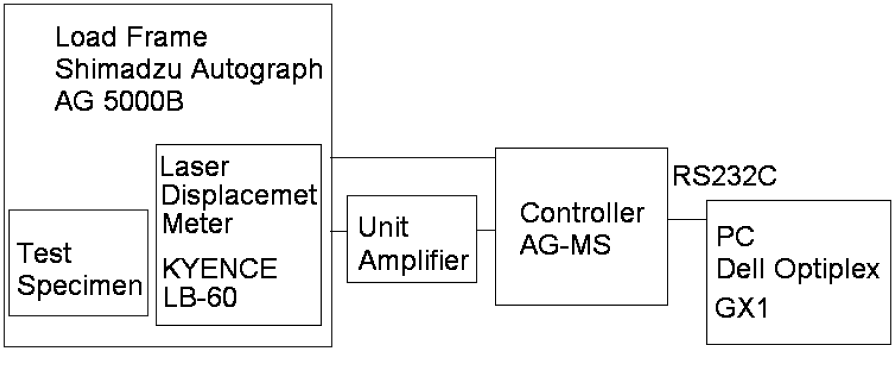

Figure 4. Measurement system.

The results showed that the influence of the attachment to the buckling load is less than 1.05%, which can be regarded as negligible for the present discussion.

5.3. Calculation of Buckling Loads

The buckling load of the experiment was calculated by Southwell's method [4]. The loading was repeated four times for each test piece. Considering the adjustment of the attachment, we used the latter three results to be averaged as an experimental

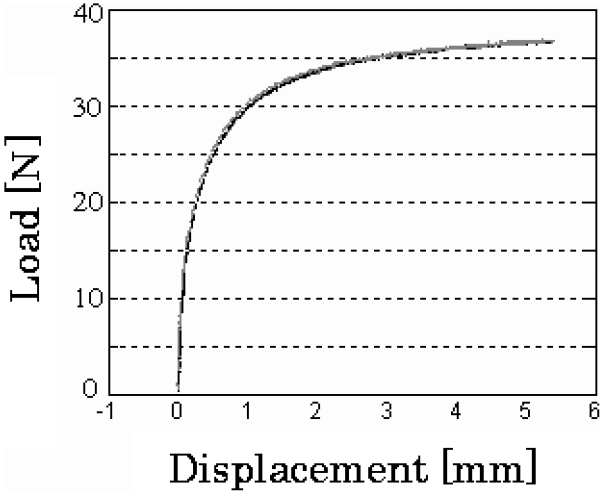

(a)

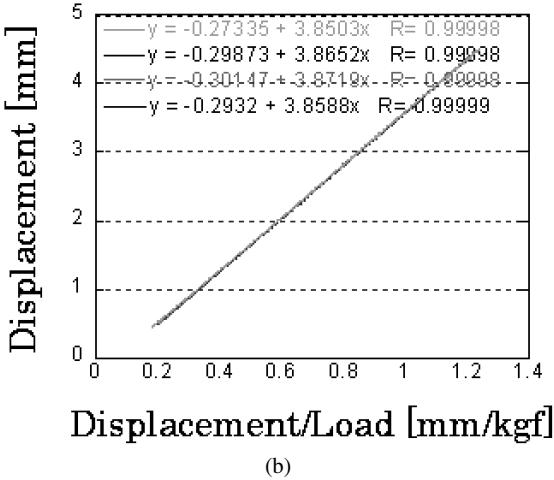

(b)

Figure 5. An example result of buckling experiments: (a) load-displacement curve of a specimen B-1 and (b) Southwell's method.

buckling load of a specimen. Furthermore, we used the higher portions of the data near the critical load, since only those parts are effective for Southwell's method.

An example of loading history for WCFP B is shown in Fig. 5(a) and its result by Southwell's method in Fig. 5(b). The data for loading, which are repeated four times, were almost on the same curve, indicating the reliability of the experimental results.

5.4. Results of the Buckling Experiments

The buckling loads were obtained with ten pieces for each material by means of the method described above. They are listed in Table 4. It can be seen with the

Table 4.
Experimental buckling loads

Materials	Buckling load P_{cr} (N)	Standard deviation σ (N)	Coefficient of variation σ/P_{cr}
GFRP L	69.8	2.79	0.040
GFRP X	36.8	1.28	0.035
GFRP T	19.0	1.10	0.058
WCFRP A	36.2	0.30	0.008
WCFRP B	37.5	0.79	0.021
Metal M	125.0	2.72	0.022

Table 5.
Comparisons between theory and experiments

Materials	Experiment P_{cr} (N)	Theory P_{th} (N)	Error P_{cr}/P_{th}
GFRP L	69.8	70.1	1.00
GFRP X	36.8	32.5	1.13
GFRP T	19.0	18.2	1.04
WCFRP A	36.2	49.9	0.73
WCFRP B	37.5	51.9	0.72
Metal M	125.0	128.0	0.98

coefficient of variation in the table that the scattering is the least for WCFP A. The buckling load itself of WCFP A is a little lower than that of WCFP B. If you compare all the materials, carbon fiber composite is almost at the same level of the coefficient of variation as the aluminum alloy, and roughly one half less than GFRP.

5.5. Comparison between Theory and Experiments

The buckling loads thus obtained by the experiments are compared with the theoretical results by Euler's buckling theory [5]:

$$P_{th} = \pi^2 EI/l^2 = \pi^2 Ebt^3/(12l^2). \tag{1}$$

The test results described in Section 4 were used as the material constants needed in the theory. The length of the beam was increased by 15.3 mm due to edge attachments. Comparisons are shown in Table 5. The results of GFRP and an aluminum alloy are in good agreement between theory and experiments. Slightly higher loads in the experiments than those of the theory are due to the effects of the stiffness of attachments and to the incompleteness of the moment-free condition at real edges. On the other hand, the difference between theory and experiments for WCFRP is large — about 28%. Although one reason for this discrepancy may arise from the elastic modulus, we examined the experimental thickness of the fabric composites,

Table 6.
Effective thickness

Test piece	Measured thickness t_m (mm)	Effective thickness t_e (mm)	Ratio t_e/t_m
BB1	1.788	1.572	0.879
BB2	1.789	1.583	0.885
BB3	1.787	1.587	0.888

since this factor was thought to be more sensitive. Surfaces of the fabric composites are wavy because of their woven fibers. In the experiments, the thickness was measured with a micrometer that measures the convex portion within the sections of sensor tips: this is likely to over-evaluate the thickness. If we assume the other measured parameters were correct, then we could calculate the thickness from the buckling load as $t = 1.63$ mm, which would be around 9% thinner. This fact suggests that we should use a concept of the effective thickness for such a composite with wavy surfaces.

In order to calculate the effective thickness t_e, additional bending and tensile tests for three WCFP B test pieces, BB1, BB2 and BB3 were conducted. First, the quantity Et^3 is calculated from the bending test by the following equation,

$$Et^3 = Wl^3/(4yb), \tag{2}$$

where W, l, y and b are the load, distance between two supports, displacement measured by a dial gauge, and width of the test piece, respectively. Next, the quantity Et is calculated from the results of tensile tests by the equation,

$$Et = W/(4y\varepsilon). \tag{3}$$

In this equation, W denotes the load, b width of a test piece and ε strain. Then, we can calculate the effective thickness using Et^3 and Et. The effective thicknesses thus obtained are listed for BB1,BB2 and BB3 in Table 6 compared with their measurements.

A ratio of the effective thickness to the measurement turned out to be 0.88. This coefficient is applied to each thickness of the specimen and then Young's modulus with the tensile tests is recalculated. The results are shown in Table 7, the values of which are much improved from those in Table 3.

5.6. Comparison Between Theory with the Corrected Modulus and Experiments

The theoretical buckling loads corrected by using both the effective thickness and the corrected modulus are compared with experiments in Table 8. It can be said from the table that the agreement is good between experimental and theoretical buckling loads with the difference of about 6%. If we assume the elastic modulus in compressive side is slightly smaller than that in tensile side, then the difference would become less. Only one case of compressive elastic modulus was re-obtained

Table 7.
Corrected elastic moduli by the effective thickness

Materials	Elastic modulus E (GPa)	Standard deviation σ (GPa)	Coefficient of variation σ/E
WCFRP A	45.0	2.96	0.066
WCFRP B	46.5	1.86	0.040

Table 8.
Comparisons of theory corrected with experiments

Materials	Experiment P_{cr} (N)	Theory P_{th} (N)	Error P_{cr}/P_{th}
WCFRP A	36.2	38.6	0.94
WCFRP B	37.5	40.1	0.94

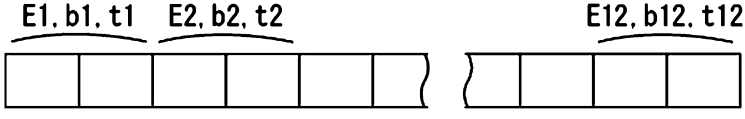

Figure 6. FEM model with 12 parameter blocks.

carefully for WCFRP B specimen. The result is that the compressive modulus is 2.6% smaller than the tensile one with the piece cut from the nearest part of the original plate. It can be said that the difference is small.

6. Numerical Simulations Considering Uncertainties

6.1. A Mathematical Model for Simulations

A beam model of the FEM is used in numerical simulations. In the analysis, the parameters E, b and t are assumed to have uncertainties while the uncertainty for the length l is neglected because of its small relative error in measurements. For each specimen, Gaussian random variables were generated so as to correspond to the coefficients of variation in the measurements as listed in Tables 1 and 2. The central limit theorem was utilized to obtain the Gaussian random variables after generating random numbers by the mixed congruential method [6]. The random variables were applied to the parameters of the finite elements of each specimen.

Next, an appropriate spatial number of blocks for uncertainties was examined by using 24 beam elements for one specimen. One thousand calculations were carried out for different sets of blocks with independent uncertainties. The number is changed as 24, 12, 6, 4, 3, 2 and 1. The case of 12 blocks is illustrated in Fig. 6.

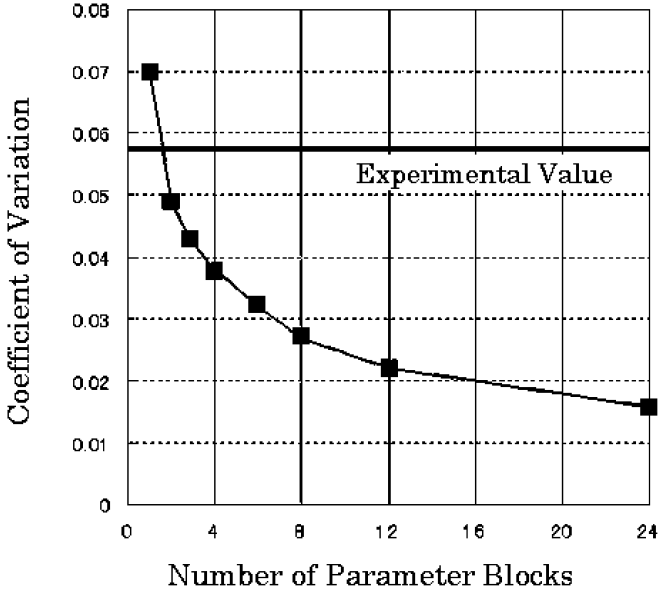

Figure 7. Coefficients of variation depending on the number of parameter blocks.

It should be noted here that the total number of elements does not have any influence on the scattering in the simulation. The scattering depends on the number of spatial blocks.

The dependence of scattering on the number of blocks as well as an experimental value of 0.058 of GFRP T is depicted in Fig. 7. The figure shows that the scattering decreases as the number of blocks increases and that the case of two blocks is the closest to the experimental value.

We also examined the actual measured data to find the appropriate number of blocks. The Fourier transform with respect to the spatial variable is applied to the measured distributions of thickness t and the width b of a specimen. The discrete Fourier transform [7] for the data sequence $\{f_0, f_1, \ldots, f_{N-1}\}$ can be given by

$$C_k = \frac{1}{N} \sum_{i=0}^{N-1} f_i \mathrm{e}^{-j(2\pi/N)ki}, \quad k = 0, 1, \ldots, N-1, \tag{4}$$

where C_k, N and j are the complex Fourier coefficient, period and imaginary unit, respectively. The symbol f_i denotes the thickness or width distribution in the present case. Since they were measured at twenty locations, N was chosen as twenty. The measured distribution of thickness with specimen X8(GFRP X) is shown in Fig. 8. The averaged Fourier coefficients for the specimens X8, X9 and X10 are shown in Fig. 9. The wave number is plotted up to ten since the coefficient will be symmetric with respect to $k = N/2$. Figure 9 indicates that the Fourier coefficient C_k is the largest at $k = 1$ with the case $k = 0$ excluded. In other words, the wave having the period N is the most dominant variation. This leads to the con-

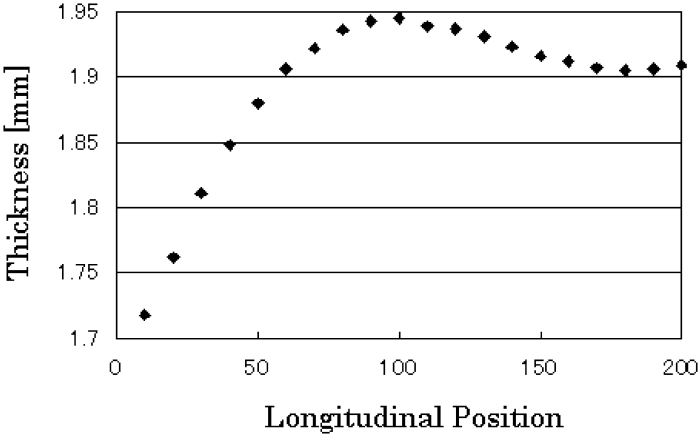

Figure 8. Thickness distribution of specimen X8.

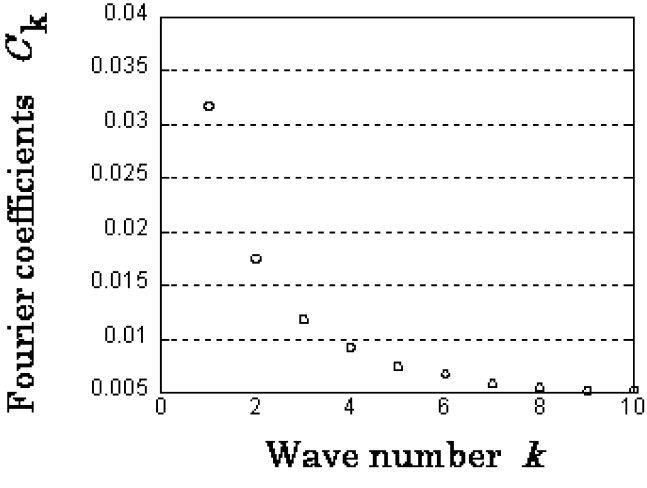

Figure 9. Averaged Fourier coefficients for X8, X9 and X10.

clusion that we should consider two blocks, one with a positive peak and the other with a negative peak.

From these results and from the further examination on the convergence with respect to the number of elements, we decided to use six elements and two blocks for numerical simulations.

6.2. Numerical Simulations and Their Results

Numerical simulations were performed with the mathematical model obtained above. One thousand buckling calculations were carried out for each specimen. The standard of deviation normalized by each averaged value, which is the coefficient of variation, is listed in Table 9.

Table 9.
Simulation results by FEM model

Materials	Buckling load P_{cr} (N)	Standard deviation σ (N)	Coefficients of variation σ / P_{cr}
GFRP L	71.0	0.90	0.013
GFRP X	32.6	1.51	0.046
GFRP T	18.1	0.88	0.049
WCFRP A	39.2	1.86	0.047
WCFRP B	40.9	1.18	0.029
Metal M	128.9	1.34	0.010

It can be seen from Table 4 and Table 9 that the scattering of the simulation is almost the same level of experimental values. The coefficients of variation for GFRP X and GFRP T are rather large when they are compared with those for Metal M.

The result of the simulation for GFRP L, however, shows a large difference from experiments. The scattering of the experimental buckling load is about twice as that of the numerical calculations. This comes from the relatively small standard deviation for the thickness of GFRP L as shown in Table 2. Equation (1) indicates that the thickness t is the most sensitive to the critical buckling load P_{cr}. Also, the limitation of the uncertainty only to E, b and t in this mathematical model can render some influence on the results. Another possible uncertainty for GFRP L may be fiber orientations.

In comparison between A and B of WCFRP, the values of the coefficient of variation are opposite with simulations and experiments. This is attributed to the fact that the result of the simulation reflects the large scattering in Young's modulus of A in the experiment, which may be caused by the uncertainty in the measurement itself. If this is true, the scattering of buckling load in the simulation for WCFRP A becomes closer to the experiment. As for WCFRP B, the simulation agrees well with the experiments. Generally, the scattering of WCFRP is favorable and close to that of the metal.

It is also pointed out from Table 4 that the experimental buckling load of B is a little larger than that for A. The result demonstrates the independence of the stub on the surfaces as far as it relates to the buckling load. But with the coefficient of deviation, B is also larger than A.

The raw data of Table 4 and Table 9 are simultaneously plotted in Fig. 10. The symbol $\circ$ corresponds to the experimental value and the symbol $\times$ indicates twenty representative results randomly obtained by the simulation. Thus, if we can evaluate the uncertainties for thickness, width, elastic modulus, and so forth for a composite specimen, then the buckling loads with proper random deviations can be estimated.

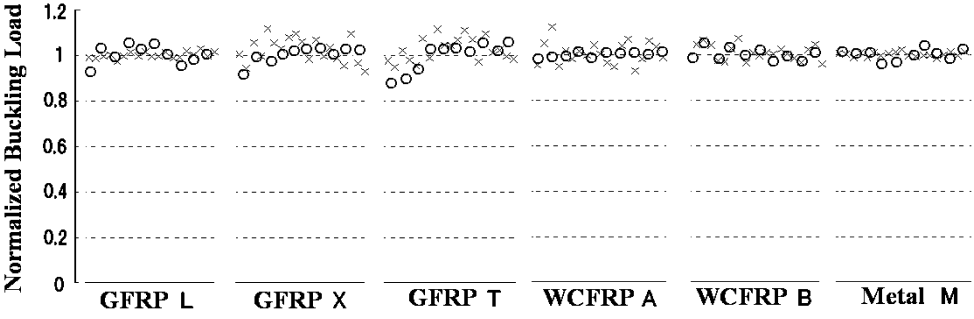

Figure 10. Test data and their numerical simulations including the effects of uncertainties.

7. Concluding Remarks

(1) Young's modulus has been measured for three types of GFRP, two types of woven CFRP and a metal.

(2) The scattering of the modulus of GFRP has a tendency to become slightly larger than that of WCFRP and of a metal.

(3) The experimental buckling load of WCFRP with stub is a little larger than that of WCFRP without stub. But for the coefficient of deviation, B is again larger than A.

(4) Firstly, the theoretical buckling load for WCFRP yields large discrepancy with the experiments. The reason was revealed to come from the measured thickness of the test piece. A correction of the theory using the additional bending and tensile tests reduced this discrepancy. This means that the introduction of 'effective thickness' is necessary to properly obtain the theoretical buckling load for WCFRP with wavy surfaces.

(5) The good agreement between the theory with corrected coefficients and the experiments is due to the fact that the newly developed attachment realizes well the condition for simple support.

(6) It is confirmed that the numerical simulation using finite elements with uncertainties provides realistic buckling loads with scattering.

References

1. M. Morita, *Composite Materials*. Nikkankougyo News Paper Pub. (1988).
2. G. Ben and T. Ishikawa, *Advanced Composite Engineering*, p. 18. Baifukan, Tokyo (2005).
3. JIS Handbook 26, Plastics Test, Japan Standard Association (2001).
4. S. Timoshenko and J. Gere, *Theory of Elastic Stability*, 2nd edn, p. 190. McGraw-Hill, New York, USA (1951).
5. S. Kobayashi, *Structural Mechanics of Aircraft*, p. 124. Maruzen, Tokyo (1992).
6. S. Ross, *Simulation*, 4th edn, pp. 27 and 42. Elsevier, New York, USA (2007).
7. S. Sato, *Introduction for Signal Analysis*, p. 103. Ohm Publishers, Tokyo (1999).